



#### **RESEARCH LETTER**

10.1029/2023GL107702

#### **Key Points:**

- It is likely that a large volcanic eruption would happen during an eventual Stratospheric Aerosol Injection (SAI) deployment
- The disruption to the stratospheric aerosol layer would require a modification of the SAI injection strategy
- We show that the hydrological impacts of a large volcanic eruption could be mitigated by such a change in strategy

#### **Supporting Information:**

Supporting Information may be found in the online version of this article.

#### Correspondence to:

I. Quaglia, iq26@cornell.edu

#### Citation:

Quaglia, I., Visioni, D., Bednarz, E. M., MacMartin, D. G., & Kravitz, B. (2024). The potential of Stratospheric Aerosol Injection to reduce the climatic risks of explosive volcanic eruptions. *Geophysical Research Letters*, *51*, e2023GL107702. https://doi.org/10.1029/2023GL107702

Received 5 DEC 2023 Accepted 3 APR 2024

#### **Author Contributions:**

Conceptualization: D. Visioni
Data curation: I. Quaglia
Formal analysis: I. Quaglia,
E. M. Bednarz
Methodology: D. Visioni
Software: I. Quaglia
Supervision: D. Visioni, D. G. MacMartin
Visualization: I. Quaglia
Writing – original draft: I. Quaglia,
D. Visioni
Writing – review & editing: D. Visioni,
E. M. Bednarz, D. G. MacMartin,

#### © 2024. The Authors.

**B** Kravitz

This is an open access article under the terms of the Creative Commons
Attribution License, which permits use, distribution and reproduction in any medium, provided the original work is properly cited.

## The Potential of Stratospheric Aerosol Injection to Reduce the Climatic Risks of Explosive Volcanic Eruptions

I. Quaglia<sup>1</sup>, D. Visioni<sup>2</sup>, E. M. Bednarz<sup>1,3,4</sup>, D. G. MacMartin<sup>1</sup>, and B. Kravitz<sup>5,6</sup>

<sup>1</sup>Sibley School of Mechanical and Aerospace Engineering, Cornell University, Ithaca, NY, USA, <sup>2</sup>Department of Earth and Atmospheric Sciences, Cornell University, Ithaca, NY, USA, <sup>3</sup>Cooperative Institute for Research in Environmental Sciences (CIRES), University of Colorado Boulder, Boulder, CO, USA, <sup>4</sup>NOAA Chemical Sciences Laboratory (NOAA CSL), Boulder, CO, USA, <sup>5</sup>Department of Earth and Atmospheric Sciences, Indiana University, Bloomington, IN, USA, <sup>6</sup>Atmospheric Sciences and Global Change Division, Pacific Northwest National Laboratory, Richland, WA, USA

**Abstract** Sulfur-rich volcanic eruptions happen sporadically. If Stratospheric Aerosol Injection (SAI) were to be deployed, it is likely that explosive volcanic eruptions would happen during such a deployment. Here we use an ensemble of Earth System Model simulations to show how changing the injection strategy post-eruption could be used to reduce the climate risks of a large volcanic eruption; the risks are also modified even without any change to the strategy. For a medium-size eruption (10 Tg-SO<sub>2</sub>) comparable to the SAI injection rate, the volcanic-induced cooling would be reduced if it occurs under SAI, especially if artificial sulfur dioxide injections were immediately suspended. Alternatively, suspending injection only in the eruption hemisphere and continuing injection in the opposite would reduce shifts in precipitation in the tropical belt and thus mitigate eruption-induced drought. Finally, we show that for eruptions much larger than the SAI deployment, changes in SAI strategy would have minimal effect.

Plain Language Summary The artificial injection of aerosols in the stratosphere (SAI) may help mitigate risks from increasing surface temperatures by reflecting some of the incoming sunlight. Such injections would need to be continued for decades, meaning that the chance is high for a sulfur-rich volcanic eruption to happen during that time. When such an eruption happens, temperatures are reduced abruptly, and there might be changes in precipitation patterns if most of the aerosols are in only one hemisphere. We show that one could envision mitigation strategy during SAI that reduce the risks arising from the abrupt changes produced by volcanic eruption, by shifting where the artificial injections happen and their amount. However, this depends on the magnitude of the eruptions, as for those too large (5 times as big as the largest eruption of the 20th century) such mitigation strategies would simply not be enough.

#### 1. Introduction

The enhancement of the stratospheric aerosol layer after explosive volcanic eruptions perturbs the energy budget of the atmosphere and oceans by reducing incoming solar radiation, and by warming the lower stratosphere. Consequently, atmospheric dynamics and ocean circulation are altered, which in turn modifies stratospheric ozone concentrations and affects the hydrologic cycle including reducing global precipitation, weakening monsoons, and shifting the position of the Inter-Tropical Convergence Zone (ITCZ) (Aquila et al., 2013; Marshall et al., 2022; Robock, 2000; Timmreck et al., 2012).

The eruption of Mt. Pinatubo in June 1991, which injected between 14 and 22 Tg of  $SO_2$  (Bluth et al., 1992; Guo et al., 2004), was estimated to produce a global cooling between 0.14 and 0.5 K in 1992–1993 (Canty et al., 2013; Dutton & Christy, 1992; Soden et al., 2002) and substantially decreased precipitation over land (Trenberth & Dai, 2007). Idealized simulations of the Pinatubo eruption within the Max Planck Institute Grand Ensemble framework show that a sulfur injection of  $\geq$ 20 Tg may lead to a significantly decreased monsoon precipitation beyond the effect of internal variability, driven by changes in atmospheric circulation (D'Agostino & Timmreck, 2022). Similar effects were also observed for smaller volcanic eruptions (e.g., 5–13 and 13 Tg of  $SO_2$  for Agung in 1963 and Santa Maria in 1902, respectively) (Textor et al., 2004; Yang et al., 2019).

The altered hemispherical thermal contrast due to the asymmetry of the zonal stratospheric aerosol distribution can shift the position of the Hadley cells and the ITCZ; the latter is pushed away from the cooler hemisphere toward the warmer one, altering regional precipitation patterns (Broccoli et al., 2006; Iles & Hegerl, 2014;

QUAGLIA ET AL. 1 of 12



10.1029/2023GL107702

Jacobson et al., 2020; Zuo et al., 2019). Through this mechanism, volcanic eruptions in the Northern Hemisphere (NH) may move the ITCZ southward and cause droughts in the Sahel region (Haywood et al., 2013; Jacobson et al., 2020), whereas Southern Hemisphere (SH) eruptions may shift the ITCZ northwards, as evidenced by the increased rainfall in Belize in the year following the Mt. Tambora eruption in 1815 (Ridley et al., 2015).

Through a similar mechanism, the increase in anthropogenic aerosol emissions in the NH since the early 1900s might have produced an asymmetric cooling between the hemispheres leading to a southward migration of the ITCZ, a drying of the northern tropics, most significant in the Sahel region, and a moistening of the southern tropics (Hwang et al., 2013).

Stratospheric Aerosol Injection (SAI) would act to mimic the mechanism behind volcanic-induced cooling by continuously injecting SO<sub>2</sub> in the lower stratosphere to temporarily offset some fraction of the greenhouse gas induced global warming (Crutzen, 2006). If the locations of the anthropogenic SO<sub>2</sub> injections are limited to one hemisphere, SAI would produce a forcing asymmetry and lead to similar changes in regional precipitation as observed for volcanic eruptions (Haywood et al., 2013; Jones et al., 2010). On the other hand, a combination of multiple injection locations results in a more even aerosol distribution and allows the management of not just global mean temperature, but also inter-hemispheric and equator-to-pole temperature gradient (Kravitz et al., 2017; Lee et al., 2020; MacMartin et al., 2017).

The length of a SAI deployment would likely range anywhere between half a century and multiple centuries, depending on the emission pathway, the desired cooling target and the timescale for the reduction of greenhouse gases concentrations (Baur et al., 2023; MacMartin et al., 2014, 2018). Since medium and large explosive eruptions are not infrequent on a centennial timescale (Schmidt et al., 2018), it is likely that under any potential SAI deployment one would occur. Thus, it is necessary to assess volcanic impacts under SAI conditions, since such an event would further affect the stratospheric aerosol layer and the resulting surface cooling.

Laakso et al. (2016) simulated a volcanic eruption of 17 Tg of SO<sub>2</sub> injected at the location of Mt. Pinatubo during a SAI deployment of a constant injection of 16 Tg-SO<sub>2</sub>/yr uniformly distributed between 30°N and 30°S. The possibility of either continuing or completely suspending the SAI deployment was considered. They found that in all simulations (with or without SAI) surface cooling and precipitation change occurred mainly in the tropics, but with different patterns depending on the background in which the eruption occurred. They also found that the volcanic-induced increase in the negative radiative forcing and the decrease in global temperature and precipitation were smaller for the eruption occurring under SAI conditions than non-SAI conditions. The non-linearity was attributed to the underlying microphysical factors that determine the responses to volcanic eruption and SAI.

Here we consider two potential kinds of eruption: one we define as "medium" magnitude ( $10 \text{ Tg-SO}_2$ ), and one as "large" magnitude ( $50 \text{ Tg-SO}_2$ ) occurring at the latitude of Pinatubo during SAI deployment, and we place ourselves upon the same SAI deployment framework as MacMartin et al. (2022), where injection amounts are latitude-dependent to manage multiple temperature-dependent degrees of freedom. We demonstrate that in such a scenario it is possible to modify the injection strategy in response to the exogenous increase in aerosol load, and that different ways of doing so come with different trade-offs. Ultimately, we show that an eruption happening under a SAI deployment leads to potentially less detectable surface impacts, and thus reduced risks, as opposed to a similar eruption happening without SAI.

#### 2. Model and Simulations

#### 2.1. The CESM2(WACCM6) Earth System Model

We use the Community Earth System Model, version 2, with the Whole Atmosphere Community Climate Model version 6 as the atmospheric component, CESM2(WACCM6) (Danabasoglu et al., 2020; Gettelman et al., 2019). CESM2(WACCM6) is a global Earth System Model that includes interactive atmosphere, ocean, land, and sea ice components, with a horizontal resolution of 0.95° latitude × 1.25° longitude, and 70 vertical layers up to ~140 km; the resolution allows a reasonable simulation of internal variability in the stratosphere (e.g., internally generated Quasi-Biennial Oscillation).

The WACCM6-MA configuration used here includes the Middle-Atmosphere (stratospheric) chemistry without representation of species and reactions that are significant only in the troposphere (Davis et al., 2023; Mills et al., 2017). Aerosols are simulated using the Modal Aerosol Model version 4 (MAM4) that includes black

QUAGLIA ET AL. 2 of 12

carbon, primary organic matter, secondary organic aerosols, sea salt, dust, and sulfate internally mixed in four lognormal modes (Primary carbon, Aitken, Accumulation, and Coarse modes) (Liu et al., 2016).

#### 2.2. Simulations

The volcanic eruptions and SAI are simulated under the Shared Socioeconomic Pathway 2–4.5 (Meinshausen et al., 2020) (SSP2-4.5) as a background greenhouse gas and anthropogenic aerosols emission scenario (MacMartin et al., 2022).

The SAI simulations are 35 years long, starting in 2035, and consist of annually constant injections of  $SO_2$  at four latitudes (30°N, 15°N, 15°S, and 30°S) all at 180°E longitude and in the gridbox centered at 21.5 km altitude (with a vertical resolution of 1.2 km). The injection rates of  $SO_2$  (Figure S1 in Supporting Information S1) are controlled by a feedback algorithm aimed at maintaining global mean temperature at 1.5°C above the preindustrial level (defined as the average over the 2020–2039 period in CESM2), and also at maintaining interhemispheric and equator-to-pole temperature gradients at the values corresponding to the same reference period (Kravitz et al., 2016; MacMartin et al., 2022). At the time of the eruption, the SAI injection rate is of 7.5 Tg- $SO_2$ /yr, with 74% located in the SH and 26% in the NH, and the mean stratospheric aerosol optical depth (sAOD) is 0.16 in SH and 0.10 in NH.

The "medium" (10 Tg-SO<sub>2</sub>) and "large" (50 Tg-SO<sub>2</sub>) volcanic eruptions are simulated both in the background scenario without SAI (Volc10Tg and Volc50Tg, respectively) and in the SAI scenario (Volc10Tg + SAI and Volc50Tg + SAI, respectively). For the case of a medium volcanic eruption, we also performed a simulation in which SAI injections are stopped in the hemisphere of the eruption and maintained in the opposite hemisphere (Volc10Tg + SAI\_nhoff). Volcanic eruptions consist of an injection uniformly distributed between 18 and 25 km altitude at the location of Mt. Pinatubo (15.1°N, 120.4°E); for simplicity, we chose the date of 1 January 2055 for the eruption. All simulations are summarized in Table S1 in Supporting Information S1.

#### 3. Results

#### 3.1. Process for SAI Strategy Determination

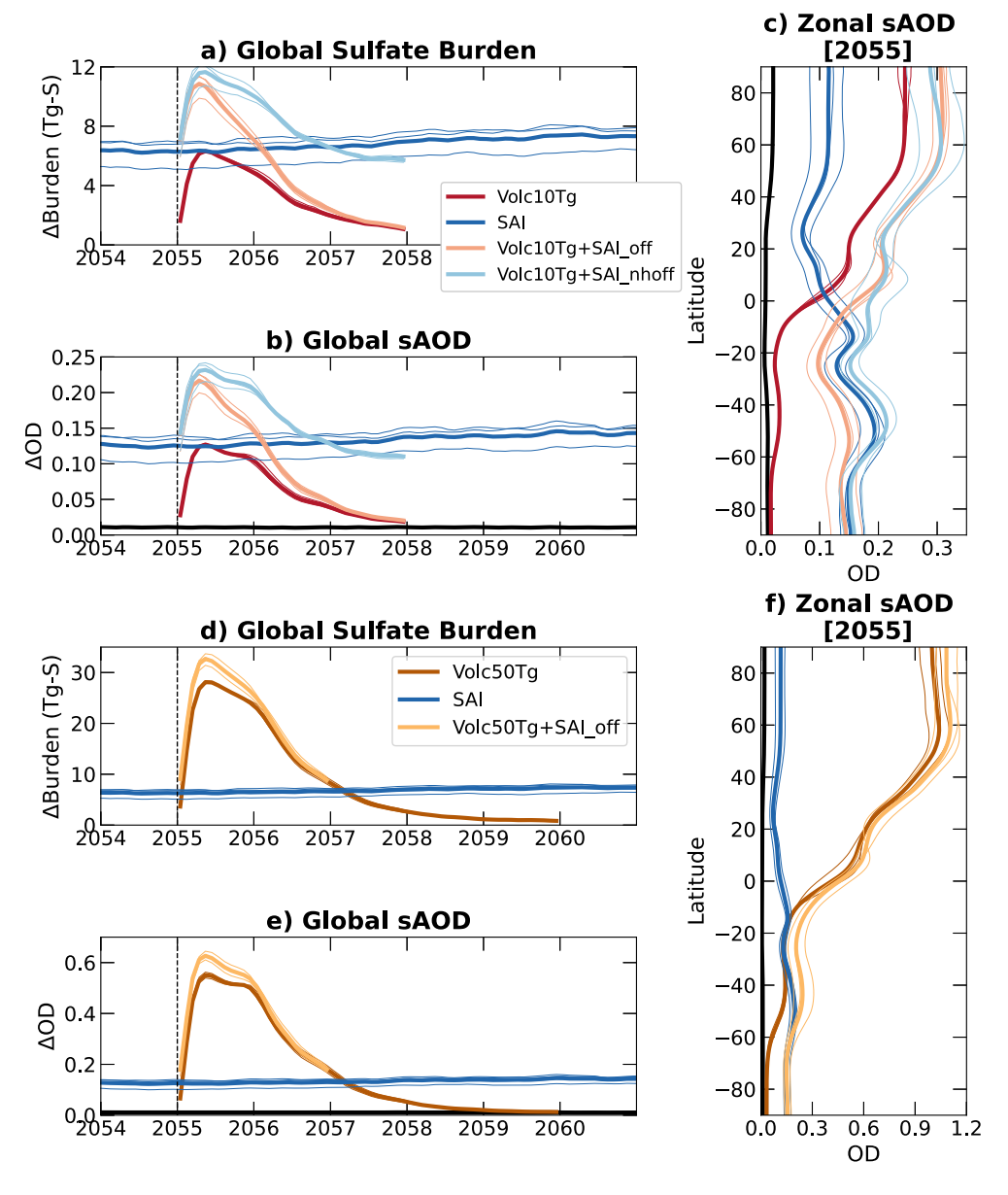
For the eruptions happening under a SAI deployment, changes to the post-eruption injection strategy are considered based on the global evolution and the latitudinal distribution of the anomalous stratospheric sulfate burden and stratospheric aerosol optical depth (sAOD) in the two eruption cases occurring under background conditions (Figure 1).

Figure 1 shows the evolution of the changes in the global sulfate burden and stratospheric aerosol optical depth with respect to SSP2-4.5, and the zonal mean changes of sAOD averaged during the first year after the eruption (2055), for both 10 Tg-SO<sub>2</sub> and 50Tg-SO<sub>2</sub> eruptions.

Both Volc10Tg and Volc50Tg global sulfate burdens and sAOD reach their maximum value 5 months after the eruption (May 2055), at 6.3 and 28.1 Tg-S for the sulfate burden and at 0.13 and 0.55 for the sAOD, respectively. Volc10 Tg values are close to the sulfate burden and sAOD achieved in the SAI simulations with no volcanic eruptions. However, all eruptions considered increase sAOD mainly in the northern hemisphere, where they occur. During the first year after the eruption when both sulfate burden and sAOD show the highest values (Figures 1c and 1f), Volc10 Tg produces an extra sAOD of 0.18 in NH (0.03 in SH); this is higher than that produced by SAI in the NH (0.10) but comparable to that in SH (0.16). For the same year, Volc50 Tg results in an extra 0.77 sAOD in the NH and 0.15 in the SH.

This latitudinal distribution of aerosols in the eruptions case suggests two possible subsequent SAI strategies based on two potential objectives: (a) to minimize the change in global mean temperature due to the eruption, one would stop all SAI injections immediately ( $Volc10Tg + SAI_off$ ,  $Volc50Tg + SAI_off$ ); (b) to minimize the changes in ITCZ due to inter-hemispheric temperature differences arising from the horizontal distribution of stratospheric aerosols, one would modify the strategy depending on the magnitude of the eruption. For objective (b), if the volcanic eruption is smaller or comparable to the amount of SAI injections (as in the case of Volc10Tg), SAI injections are either reduced or stopped in the hemisphere of eruption and maintained in the opposite hemisphere ( $Volc10Tg + SAI_nhoff$ ). If it is larger, the injection should be increased in the opposite hemisphere, since stopping the injection in the eruption hemisphere would not yield an appreciable change in the hemispheric

QUAGLIA ET AL. 3 of 12



**Figure 1.** Monthly values of globally averaged sulfate burden change and stratospheric aerosol optical depth. (a, d) Globally averaged sulfate burden change with respect to SSP2-4.5 for 10 Tg and 50 Tg of SO<sub>2</sub> eruption, respectively. (b, e) Globally averaged stratospheric aerosol optical depth for 10 Tg and 50 Tg of SO<sub>2</sub> eruption, respectively. (c, f) Zonal aerosol optical depth averaged over 2055 for 10 Tg and 50 Tg of SO<sub>2</sub> eruption, respectively.

asymmetry of AOD. However, for our large eruption case this would likely have significant adverse impacts on global mean temperature and precipitation, and as such is unlikely to represent a plausible mitigation strategy. Therefore, for the Volc50Tg case, we only consider stopping SAI everywhere following the eruption (Volc50Tg + SAI\_off). A third strategy would consist of keeping SAI injection unchanged despite the eruption, but that would not bring additional benefits and therefore we do not consider it here.

The changes in sulfate aerosol burden and sAOD due to volcanic eruptions are smaller, and their lifetime is shorter, when the eruption occurs during SAI (Volc10Tg + SAI\_off and Volc50Tg + SAI\_off) than under SSP2-4.5 (Volc10Tg and Volc50Tg) (Figures 1b and 1e). This happens both because SAI injections are suspended posteruption and because the injection of  $SO_2$  on top of a perturbed stratospheric aerosol layer enhances aerosol

QUAGLIA ET AL. 4 of 12

1944807. 2024. 8, Downloaded from https://agupubs.onlinelibrary.wiey.com/doi/10.1092/2023GL107702. Wiley Online Library on [0705/2024]. See the Terms and Conditions (https://onlinelibrary.wiley.com/rerms-and-conditions) on Wiley Online Library for rules of use: OA articles are gow

growth since condensation would prevail over nucleation, resulting in larger aerosols and, in turn, faster sedimentation (Laakso et al., 2016; Visioni et al., 2019; Yu et al., 2023).

For the same reasons, the stratospheric sulfate burden and aerosol optical depth returns to pre-eruption levels significantly slower under SSP2-4.5 than under SAI, taking about 3 years in total. For the medium eruption (10 Tg-SO<sub>2</sub>) under SAI, the global sulfate burden and sAOD take 1 year to return to the pre-eruption SAI values if SAI is suspended everywhere, and around 2 years if SAI is suspended only in the hemisphere of eruption. For the large eruption (50 Tg-SO<sub>2</sub>) occurring under SAI, where the SAI is suspended everywhere, two years are necessary for the stratospheric aerosols to return to the pre-eruption levels.

 $Volc10Tg + SAI_{off}$  and  $Volc50Tg + SAI_{off}$  are run for the duration it takes for the stratospheric aerosol burden to reach roughly the same levels as for the eruption under SSP2-4.5, which is around 2 and 3 years respectively, to investigate the e-folding time. In  $Volc10Tg + SAI_{off}$ , the NH SAI injections are restarted 2 years after the eruption to allow the global sulfate burden and sAOD to converge to pre-eruption values. In that case, during the first year after the eruption, stopping the injection only in the NH results in a more symmetrical inter-hemispheric distribution of sAOD than the case where SAI is suspended everywhere; it does, however result in a higher global sAOD. The climatic-trade-offs between these two cases will be analyzed in the next sections.

#### 3.2. Global Changes in Temperatures

The three degrees of freedom for near-surface air temperatures (defined in Appendix A) that are being managed by the multi-location SAI strategy are: global mean temperature (GMT,  $T_0$ ) in Figure 2a, the inter-hemispheric temperature gradient ( $T_1$ ), and the equator-to-pole temperature gradient ( $T_2$ ) in Figures S2a and S2b in Supporting Information S1, respectively.

Figure 2a shows that SSP2-4.5 GMT increases over the 21st century at a rate of 0.3 K decade<sup>-1</sup>, but is held at  $1.5 \pm 0.1$  K above preindustrial levels under SAI. Following each eruption under SSP2-4.5, a cooling of 0.3 and 1.1 K in Volc10Tg and Volc50Tg is simulated (2055–2056 average). The volcanic contribution to GMT is 0.1 K smaller when SAI is stopped in one hemisphere (Volc10Tg + SAI\_nhoff) and 0.2 K smaller for either eruption happening under SAI when stopped everywhere. GMT returns to the respective background values in SSP2-4.5 after 3 years for Volc10Tg and 5 years for Volc50Tg. Under SAI, the return time for GMT depends on the strategy: if artificial SO<sub>2</sub> injections are suspended everywhere it takes about 2 years less in either cases than under SSP2-4.5, whereas if the injections are maintained in one hemisphere the return time is similar to that under SSP2-4.5.

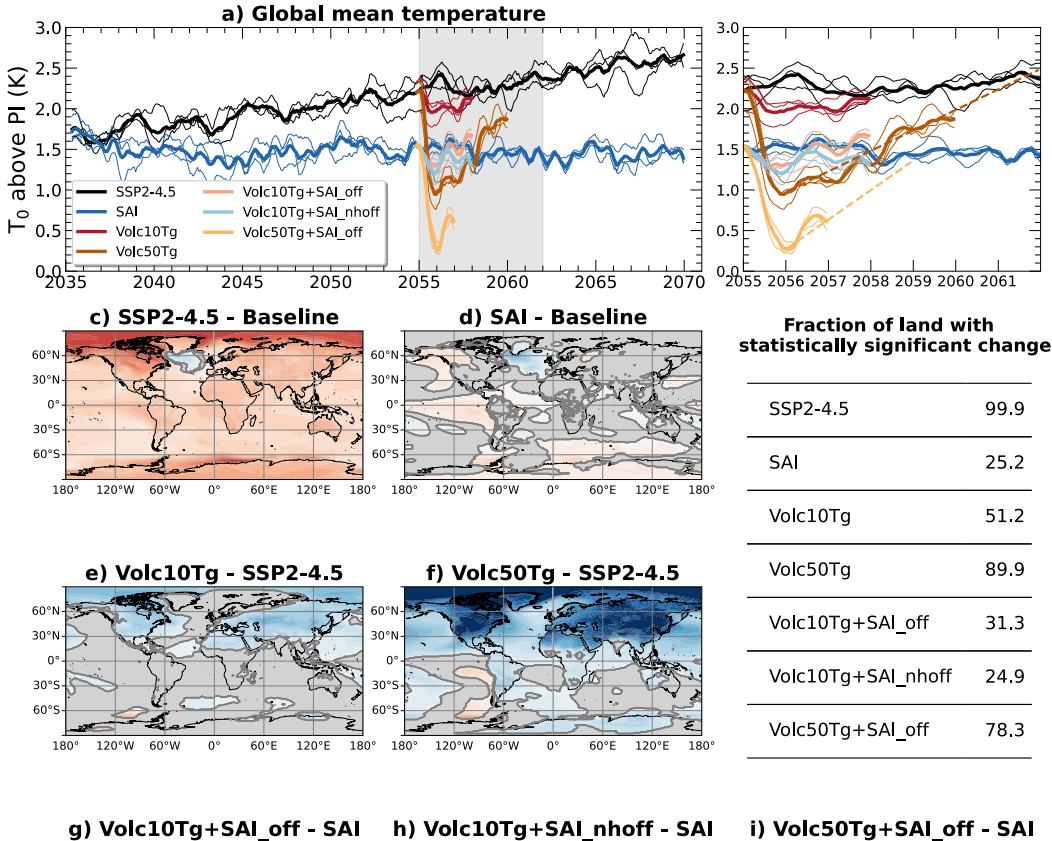
While both SSP2-4.5 and SAI maintain a roughly constant inter-hemispheric temperature gradient (0.93  $\pm$  0.07 K in SSP2-4.5 and at 0.84  $\pm$  0.06 K in SAI, Figure S2a in Supporting Information S1, all simulations with volcanic eruptions mainly cool the NH and thus result in the reduction of values of  $T_1$ . All of the cases with a medium-size eruptions lead to a similar decrease in  $T_1$  in the two following years: 0.75  $\pm$  0.7 K in Volc10Tg, 0.72  $\pm$  0.07 K Volc10Tg + SAI\_off and 0.73  $\pm$  0.07 K Volc10Tg + SAI\_nhoff. The large size (50 Tg SO<sub>2</sub>) eruptions lead to much lower values of  $T_1$  (lowest value of 0.13 in Volc50Tg and 0.14 K in Volc50Tg + SAI\_off) and a subsequent return toward higher values at a rate of about 1.25 K/year.

In Figure S2b in Supporting Information S1, the equator-to-pole temperature gradient increases (becomes less negative) in SSP2-4.5 from 2035 at a rate of 0.03 K/decade due to Arctic amplification, while under SAI it stays at around  $-5.89 \pm 0.06$  K. After the volcanic eruptions, a larger cooling in the northern extratropics compared to the tropics leads to a decrease in  $T_2$  by 0.1 and 0.3 K for the 10 and 50 Tg-SO<sub>2</sub> eruptions compared to the respective background, with a slightly smaller decrease in Volc10Tg + SAI\_nhoff and Volc50Tg + SAI\_off.

#### 3.3. Regional Changes in Temperatures

In Figures 2b–2h we show the regional distribution of temperature changes, only highlighting regions where the differences are statistically significant at the 95% significance level (see Appendix B). Panels 2b and c show the temperature change in SSP2-4.5 and SAI in 2050–2069 compared to the 20-year average over 2020–2039 in SSP2-4.5 (Baseline). The increase in greenhouse gas concentrations in SSP2-4.5 results in a warming over almost the entire globe except for a region in the North Atlantic Ocean due to a projected continued slowdown of the Atlantic Meridional Overturning Circulation (see Figure 3 in MacMartin et al. (2022); see also Gervais et al. (2018)). A higher warming compared to the global mean is evident in the Arctic region (1.8 K) due to Arctic

QUAGLIA ET AL. 5 of 12



SAT change

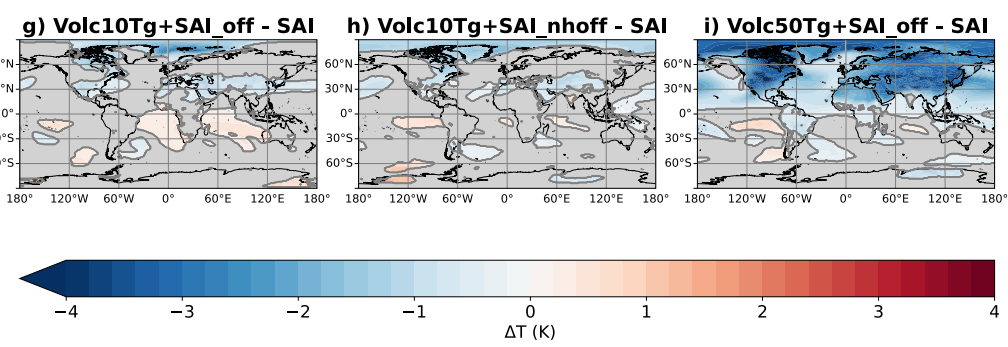


**Figure 2.** (a) Time series of monthly mean of global temperature  $(T_0)$  in K above preindustrial levels (PI) from 2035 to 2070 (left) and zoom in (right) on years highlighted by gray box.  $T_0$  is a 12-month rolling mean over 12 months and deseasonalized by subtracting detrended background values with a linear fit over the years 2035–2069. (b–h) Maps of statistically significant change of temperature from different background simulation based on the considered simulation. Gray areas are the region where the differences are non statistically significant at the 5% significance level. (b, c) Show the temperature change in SSP2-4.5 and SAI averaged over 2050–2069 from Baseline (SSP2-4.5 averaged over 2020–2039) and the statistics are calculated over all the simulation years for the three ensemble members. (d, e) As (b, c) for Volc10 Tg and Volc50 Tg averaged over 2055–2056 from the 20-year average in SSP2-4.5. (f–h) As (b, c) for Volc10Tg + SAI\_off, Volc10Tg + SAI\_nhoff and Volc50Tg + SAI\_off averaged over 2055–2056 from the 20-year average in SAI.

amplification with associated reduction in September sea ice (Figure S3 in Supporting Information S1, black line). Under SAI, the injection was not quite sufficient to meet the desired target temperature, leading to a residual warming relative to Baseline of 0.1 K (globally averaged) and a fraction of land with statistically significant change of 25.2% versus the of 0.9 K and 99.9% in SSP2-4.5.

In Figures 2d and 2e we show the temperature change over the 2 years following the eruptions compared to the 20-year average in SSP2-4.5 (2050–2069); likewise, Figures 2f–2h show the changes for the eruptions occurring

QUAGLIA ET AL. 6 of 12



10.1029/2023GL107702

under SAI (Volc10Tg + SAI\_off, Volc10Tg + SAI\_nhoff, Volc50Tg + SAI\_off) compared to the 20-year average in the SAI case without eruptions. Unlike for panels b and c), here we aim to highlight the direct perturbation produced by the eruption compared to the simulated climatology: shaded areas here are meant to indicate regions where the change produced by the eruption are not significant compared to the variability (considered here as the standard error calculated over 20 years and three ensemble members) over a longer climatological period.

As discussed before, the eruptions mainly decrease near-surface air temperatures in the hemisphere of the eruption; however, the temperature change compared to the respective background is significantly smaller when the eruptions occur during SAI (Figures 2d and 2e compared to Figures 2f–2h). The average cooling from the eruption in the NH is 0.6 K in Volc10Tg and 2.0 K in Volc50Tg (Figures 2d and 2e); this is 0.4 K smaller, regardless of the eruption magnitude, when occurring under SAI (Figures 2f–2h). Furthermore, the fraction of land with statistically significant temperature changes from the background is lower for eruptions occurring under SAI background, as shown in the table in Figure 2.

#### 3.4. Precipitation and ITCZ Shift

Variations in global surface temperatures affect global precipitation, and variations in the inter-hemispheric thermal contrast affect the location of the tropical Hadley circulation, including the location of the ITCZ, in turn resulting in changes in the regional distribution of precipitation.

The most significant changes in precipitation occur over the Tropics, as shown in Figure 3 (calculated as in Figure 2). Global warming (Figure 3a) produces an increase in precipitation around the equator in the Pacific Ocean, in the Atlantic Ocean extending over Brazil and regions of west-central Africa, and over a small eastern region on the Indian Ocean facing east-central Africa; above these regions, a drying belt extends into the northern tropic. In our simulations, the overall change in precipitation is statistically significant over 29.9% of land areas. This percentage decreases to 14.0% when SAI is deployed.

The clear hydrological response from volcanic eruptions (Figures 3c–3g), driven mainly by changing interhemispheric temperature gradients resulting in a southward shift of ITCZ, is a decrease in precipitation in the northern tropics and an increase in the southern tropics; these changes are larger and more statistical significant in the case of the larger eruption. If injections are stopped everywhere (Figures 3e and 3g), the fraction of land affected by the change in precipitation (see table in Figure 3) and the magnitude of precipitation changes over land are comparable (medium eruption) or only slightly attenuated (large eruption) with respect to those occurring under SSP2-4.5 (Figures 3c and 3d); however, if injections are maintained in the opposite hemisphere (Figure 2f), then these changes are reduced.

In Figure 3h, the annual mean position of the ITCZ is calculated as the latitude near the equator where the meridional mass stream function at 500 hPa changes sign, and the shift is calculated compared to the ITCZ position in Baseline (mean value over the reference period, 2020–2039). For volcanic eruptions, with or without SAI, the decrease in inter-hemispheric temperature gradient about a year after the eruption forces a southward shift of ITCZ. The ITCZ shift is  $-4.4^{\circ}$  in Volc10Tg and decreases to  $-3.0^{\circ}$  in Volc10Tg + SAI\_off and further to  $-2.6^{\circ}$  in Volc10Tg + SAI\_nhoff. Similarly, the ITCZ shift is larger in Volc50 Tg, with a shift of  $-8.2^{\circ}$  without SAI, decreasing to  $-7.3^{\circ}$  for Volc50Tg + SAI\_off.

Finally, we focus our analyses on two regions within the tropical belt in which precipitation changes during the monsoon season might be of particular interest and has been demonstrated to be affected by volcanic eruptions in the past (Haywood et al., 2013): the Sahelian region and the Indian subcontinent (Figure 4). As shown in Figures 4c and 4d, precipitation is reduced in these regions in late summer and early autumn under a medium size eruption occurring under SSP2-4.5. In contrast, limiting the ITCZ shift by a change in the SAI injection strategy post-eruption, especially in the case when the injections are suspended only the in the NH, results in a significant amelioration of the volcanic-induced precipitation reduction and, thus, potentially, food and water security.

#### 4. Conclusion

If SAI is ever deployed, it is highly likely that it would have to be maintained over many decades to centuries (Baur et al., 2023; Ricke et al., 2017): it is therefore also highly likely that, given the frequency of large-magnitude volcanic eruptions, one might happen during a deployment, underscoring both the importance of assessing the

QUAGLIA ET AL. 7 of 12

## **Precipitation change**

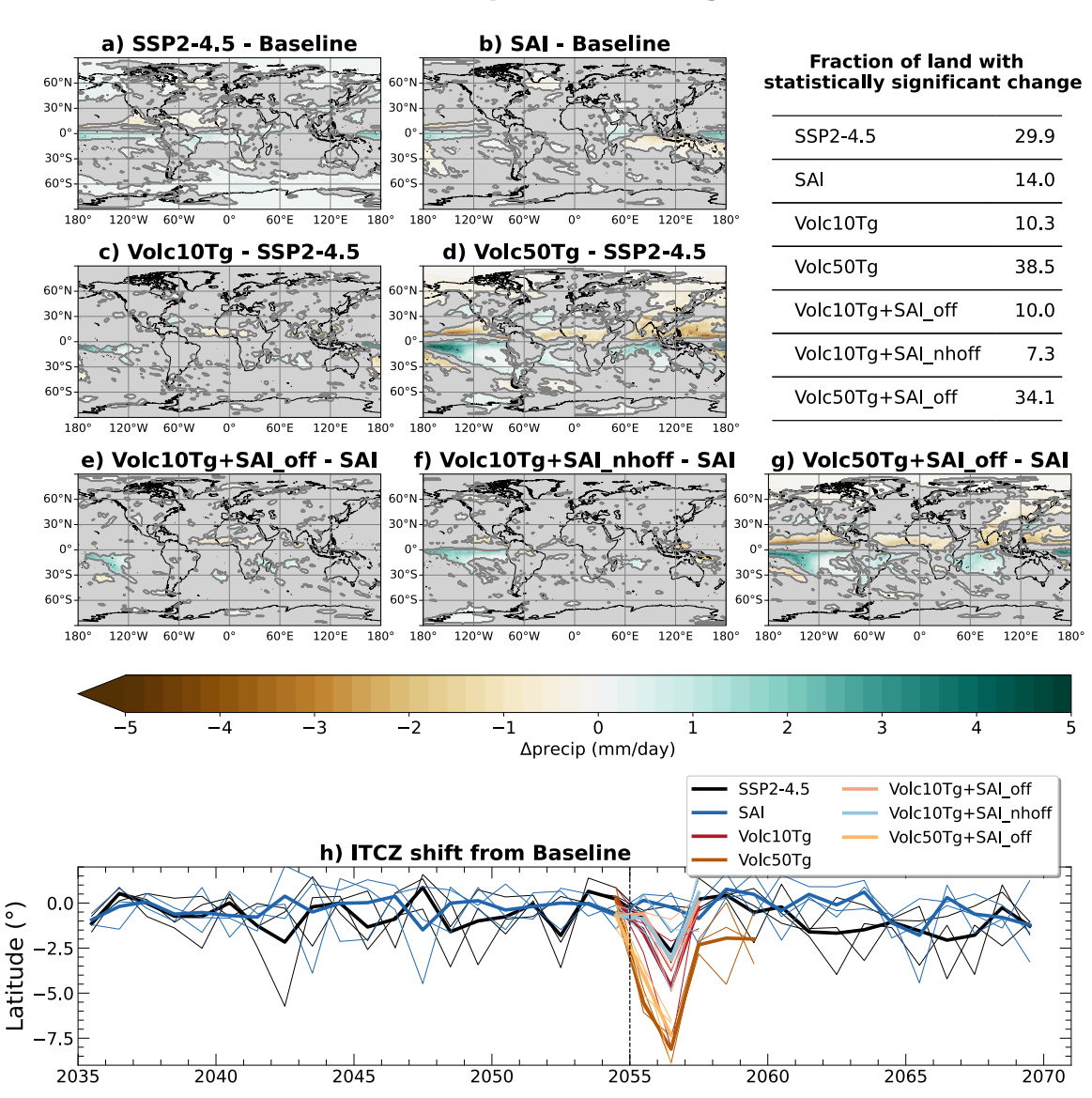


Figure 3. Maps of statistically significant changes in precipitation as a deviation from the respective background simulation. Gray areas indicate regions where the differences are not statistically significant at the 5% level. (a, b) Show the precipitation change in SSP2-4.5 and SAI averaged over 2050–2069 from Baseline (SSP2-4.5 averaged over 2020–2039) and the statistics are calculated over all the simulation years for the three ensemble members. (c, d) As (a, b) for Volc10 Tg and Volc50 Tg averaged over 2055–2056 from the 20-year average in SSP2-4.5. (e–g) As (a, b) for Volc10 Tg + SAI\_off, Volc10 Tg + SAI\_nhoff and Volc50 Tg + SAI\_off averaged over 2055–2056 from the 20-year average in SAI. (h) Time series of annual mean of the ITCZ shift with respect to ITCZ position in Baseline. ITCZ position in Baseline is calculated as the average position of the ITCZ in SSP2-4.5 over the reference period (2020–2039).

combined effects of the two and of better understanding the future frequency of sulfur-rich volcanic eruptions (Carn et al., 2017; Galetto et al., 2023; Schmidt et al., 2018).

The decrease of the hemispheric and land-ocean thermal contrast after an explosive volcanic eruption, due to the differential cooling of one hemisphere, weakens the cross-equatorial flow and consequently shifts the ITCZ position, causing drying and wetting of the climatological wet and dry regions, respectively (Haywood et al., 2013; Iles & Hegerl, 2014; Zuo et al., 2019).

In this work we have therefore asked the question of how the two increases of stratospheric loading, one pulse-like from a volcanic eruption and one sustained from a SAI deployment, would interact. In particular, we consider a

19448007, 2024, 8, Downloaded from https://agupubs.onlinelibrary.wiley.com/doi/10.1029/2023GL107702, Wiley Online Library on [07/05/2024]. See the Terms and Conditions (https://onlinelibrary.wiley.com/terms

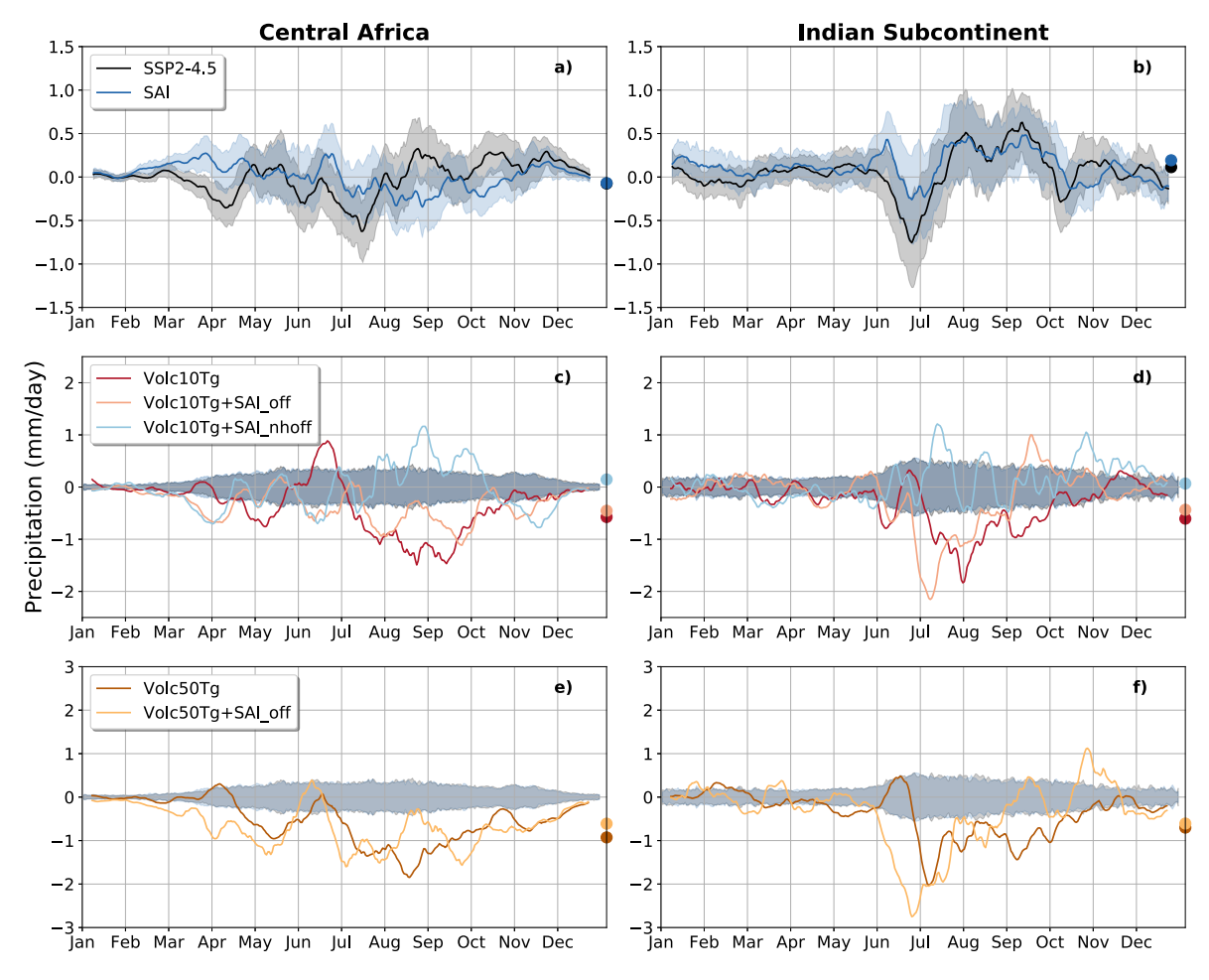


Figure 4. Precipitation change calculated over the Sahelian (left) and Indian (right) regions as defined in Figure S4 in Supporting Information S1. (a, b) Changes compared to Baseline for SSP2-4.5 and SAI. Shadings represent ± one standard error considering three ensemble members and 20 years. (c, d) Changes compared to the respective background cases (SSP2-4.5 and SAI) under a 10 Tg volcanic eruption. (e, f) Changes compared to the respective background cases under a 50 Tg volcanic eruption. In panels (c-f), the shading indicates the variability in the long-term, 20 years response as in (a, b), but is here centered around 0 to indicate if the volcanic-produced changes fall outside of the long-term variability. The circles on the right axis represent the average values over the summer monsoon (MJJAS).

SAI injection strategy that consider multiple injection locations in both hemisphere, to prevent not just a global mean temperature increase but also an imbalance in the rates of warming between hemisphere. In this context, we simulate two volcanic eruptions with either 10 or 50 Tg of SO<sub>2</sub> at a location close to 15°N in 2055 (after 20 years of SAI deployment).

Without an SAI deployment, and lacking any means to artificially reduce the stratospheric aerosol load, there is little that can be done to counteract the adverse climatic effects of a volcanic eruption. During a coordinated (and thus controllable) SAI deployment, on the other hand, we can consider potential responses to volcanic eruptions by means of modifying the SAI injection strategy. In this work, we consider as an example two possible response strategies: one that aims to minimize the overall excessive cooling caused by the volcanic eruption, and one that prioritizes preventing a thermal imbalance between the hemisphere, insuring that the aerosol load is balanced between the hemispheres. The first case involves stopping SAI injections everywhere, regardless of the spatial and temporal evolution of volcanic plume. In contrast, the latter defines the modification of the second SAI strategy based on what we first observed for a volcanic eruption in a non-SAI background. We note that in general a volcanic eruption in one hemisphere tends to perturb the aerosol layer mainly in the hemisphere of eruption (Oman et al., 2006; Schoeberl et al., 2023; Self, 2006). In a real-world deployment, one could further constrain the post-eruption evolution of a volcanic plume, and thus the particulars of SAI strategy that need to be modified, using parallel forecast model simulations.

In the eruption cases we consider here, the SAI deployment by 2055 is comparable in magnitude to the smaller one; this means that injections can either be stopped everywhere for that year, for the first strategy, or be completely stopped only in the same hemisphere as the eruption, and continued as planned in the other, for the second strategy. In the former case, we demonstrate that the post-eruption abrupt global cooling can be reduced compared to the case without SAI by 67%; in the latter, we demonstrate that the post-eruption hydrological changes in the tropical belt (in particular in specific regions that might be particularly sensitive to changes in the monsoonal season, such as Central Africa and the Indian Subcontinent) can be minimized compared to the case without SAI. For the eruption case that is much larger than the SAI deployment, we provide a strategy where SAI injections are stopped everywhere, and which manages to partially reduces the post-eruption abrupt global cooling by 17% and minimizes changes over 11% of the land. However, we argue that a strategy that aims to prevent an hemispheric imbalance would not be feasible as it would overcool too much compared by the cooling already provided by the volcanic eruption. Nonetheless, even the case where injections are completely stopped offers some reduction in the hydrological changes produced by the 50 Tg of SO<sub>2</sub> eruption.

More generally, our considerations can be applied whenever considering volcanic eruptions with sulfate loading smaller or comparable to a certain SAI injection rate: we demonstrated that in those cases injection strategy considerations could affect, and for the aspects considered here, minimize, post-eruption risks. For eruptions much larger than SAI injection rates, we demonstrate that the concurrence of SAI and eruption would, at the very least, not increase climatically relevant risks as argued elsewhere (Tang & Kemp, 2021), and potentially reduce them just by reducing the resulting abrupt cooling.

### **Appendix A: Temperature Metrics**

Global mean temperature (GMT,  $T_0$ ), the inter-hemispheric temperature gradient ( $T_1$ ), and the equator-to-pole temperature gradient ( $T_2$ ) are defined as follows based on Kravitz et al. (2016):

$$T_0 = \frac{1}{A} \int_{\Psi} T(\Psi) \cos(\Psi) d\Psi \tag{A1}$$

$$T_1 = \frac{1}{A} \int_{\Psi} \sin(\Psi) T(\Psi) \cos(\Psi) d\Psi \tag{A2}$$

$$T_2 = \frac{1}{A} \int_{\Psi} \frac{3\sin^2(\Psi) - 1}{2} T(\Psi) \cos(\Psi) d\Psi$$
 (A3)

where  $T(\Psi)$  is zonal-mean temperature,  $\Psi$  is latitude, and A is area-weighted latitude.

#### **Appendix B: Temperature and Precipitation Changes**

The statistically significant changes in temperature and precipitation are calculated at the 95% level of significance and considering three ensemble members. The number of years and the background scenario against which changes and statistics are calculated is always explicitly discussed in the figure captions and in the text; often, when considering changes in SSP2-4.5 and SAI, the comparison considers averages over 2050–2069 as compared with the Baseline period (always defined as SSP2-4.5 averaged over 2020–2039); when considering changes in Volc10Tg and Volc50Tg, we use the period 2055–2056 against the 20-year average in SSP2-4.5 (2050–2069); in Volc10Tg + SAI\_off, Volc10Tg + SAI\_nhoff and Volc50Tg + SAI\_off we consider an average over 2055–2056 against the 20-year average in SAI (2050–2069).

#### **Conflict of Interest**

The authors declare no conflicts of interest relevant to this study.

#### **Data Availability Statement**

Simulation data used in this work are available in Quaglia (2023).

QUAGLIA ET AL. 10 of 12



10.1029/2023GL107702

#### Acknowledgments

We would like to acknowledge highperformance computing support from Cheyenne (https://doi.org/10.5065/ D6RX99HX) provided by NCAR's Computational and Information Systems Laboratory, sponsored by the National Science Foundation. Support for IQ, DV, and DGM was provided by the Atkinson Center for a Sustainability at Cornell University and by the National Science Foundation through agreement CBET-2038246. Support for EMB was provided by the NOAA cooperative agreement NA22OAR4320151, and the NOAA Earth's Radiative Budget initiative. Support for BK was provided in part by the National Science Foundation through agreement SES-1754740, NOAA's Climate Program Office, Earth's Radiation Budget (ERB) (Grant NA22OAR4310479), and the Indiana University Environmental Resilience Institute.

#### References

- Aquila, V., Oman, L. D., Stolarski, R., Douglass, A. R., & Newman, P. A. (2013). The response of ozone and nitrogen dioxide to the eruption of Mt. Pinatubo at southern and northern midlatitudes. *Journal of the Atmospheric Sciences*, 70(3), 894–900. https://doi.org/10.1175/JAS-D-12-0143.1
- Baur, S., Nauels, A., Nicholls, Z., Sanderson, B. M., & Schleussner, C.-F. (2023). The deployment length of solar radiation modification: An interplay of mitigation, net-negative emissions and climate uncertainty. *Earth System Dynamics*, 14(2), 367–381. https://doi.org/10.5194/esd-14-367-2023
- Bluth, G. J. S., Doiron, S. D., Schnetzler, C. C., Krueger, A. J., & Walter, L. S. (1992). Global tracking of the SO<sub>2</sub> clouds from the June, 1991 Mount Pinatubo eruptions. Geophysical Research Letters, 19(2), 151–154. https://doi.org/10.1029/91GL02792
- Broccoli, A. J., Dahl, K. A., & Stouffer, R. J. (2006). Response of the ITCZ to Northern Hemisphere cooling: ITCZ response to N. Hemisphere cooling. Geophysical Research Letters, 33(1). https://doi.org/10.1029/2005GL024546
- Canty, T., Mascioli, N. R., Smarte, M. D., & Salawitch, R. J. (2013). An empirical model of global climate—Part 1: A critical evaluation of volcanic cooling. Atmospheric Chemistry and Physics, 13(8), 3997–4031. https://doi.org/10.5194/acp-13-3997-2013
- Carn, S. A., Fioletov, V. E., McLinden, C. A., Li, C., & Krotkov, N. A. (2017). A decade of global volcanic SO<sub>2</sub> emissions measured from space. Scientific Reports, 7(1), 44095. https://doi.org/10.1038/srep44095
- Crutzen, P. (2006). Albedo enhancement by stratospheric sulfur injections: A contribution to resolve a policy dilemma? *Climatic Change*, 77(3), 211–220. https://doi.org/10.1007/s10584-006-9101-y
- D'Agostino, R., & Timmreck, C. (2022). Sensitivity of regional monsoons to idealised equatorial volcanic eruption of different sulfur emission strengths. Environmental Research Letters, 17(5), 054001. https://doi.org/10.1088/1748-9326/ac62af
- Danabasoglu, G., Lamarque, J.-F., Bacmeister, J., Bailey, D. A., DuVivier, A. K., Edwards, J., et al. (2020). The Community Earth System Model Version 2 (CESM2). Journal of Advances in Modeling Earth Systems, 12(2), e2019MS001916. https://doi.org/10.1029/2019MS001916
- Davis, N. A., Visioni, D., Garcia, R. R., Kinnison, D. E., Marsh, D. R., Mills, M., et al. (2023). Climate, variability, and climate sensitivity of "middle atmosphere" chemistry configurations of the Community Earth System Model Version 2, Whole Atmosphere Community Climate Model Version 6 (CESM2(WACCM6)). Journal of Advances in Modeling Earth Systems, 15(9), e2022MS003579. https://doi.org/10.1029/2022MS003579
- Dutton, E. G., & Christy, J. R. (1992). Solar radiative forcing at selected locations and evidence for global lower tropospheric cooling following the eruptions of El Chichón and Pinatubo. *Geophysical Research Letters*, 19(23), 2313–2316. https://doi.org/10.1029/92GL02495
- Galetto, F., Pritchard, M. E., Hornby, A. J., Gazel, E., & Mahowald, N. M. (2023). Spatial and temporal quantification of subaerial volcanism from 1980 to 2019: Solid products, masses, and average eruptive rates. Reviews of Geophysics, 61(1), e2022RG000783. https://doi.org/10.1029/ 2022RG000783
- Gervais, M., Shaman, J., & Kushnir, Y. (2018). Mechanisms governing the development of the North Atlantic warming hole in the CESM-le future climate simulations. *Journal of Climate*, 31(15), 5927–5946. https://doi.org/10.1175/JCLI-D-17-0635.1
- Gettelman, A., Mills, M. J., Kinnison, D. E., Garcia, R. R., Smith, A. K., Marsh, D. R., et al. (2019). The Whole Atmosphere Community Climate Model Version 6 (WACCM6). *Journal of Geophysical Research: Atmospheres*, 124(23), 12380–12403. https://doi.org/10.1029/2019ID030943
- Guo, S., Bluth, G. J. S., Rose, W. I., Watson, I. M., & Prata, A. J. (2004). Re-evaluation of SO<sub>2</sub> release of the 15 June 1991 Pinatubo eruption using ultraviolet and infrared satellite sensors. *Geochemistry, Geophysics, Geosystems*, 5(4), Q04001. https://doi.org/10.1029/2003GC000654
- Haywood, J. M., Jones, A., Bellouin, N., & Stephenson, D. (2013). Asymmetric forcing from stratospheric aerosols impacts Sahelian rainfall. Nature Climate Change, 3(7), 660–665. https://doi.org/10.1038/nclimate1857
- Hwang, Y., Frierson, D. M. W., & Kang, S. M. (2013). Anthropogenic sulfate aerosol and the southward shift of tropical precipitation in the late 20th century. *Geophysical Research Letters*, 40(11), 2845–2850. https://doi.org/10.1002/grl.50502
- Iles, C. E., & Hegerl, G. C. (2014). The global precipitation response to volcanic eruptions in the CMIP5 models. *Environmental Research Letters*, 9(10), 104012. https://doi.org/10.1088/1748-9326/9/10/104012
- Jacobson, T. W. P., Yang, W., Vecchi, G. A., & Horowitz, L. W. (2020). Impact of volcanic aerosol hemispheric symmetry on Sahel rainfall. Climate Dynamics, 55(7–8), 1733–1758. https://doi.org/10.1007/s00382-020-05347-7
- Jones, A., Haywood, J., Boucher, O., Kravitz, B., & Robock, A. (2010). Geoengineering by stratospheric SO<sub>2</sub> injection: Results from the Met Office HadGEM2 climate model and comparison with the Goddard Institute for Space Studies ModelE. *Atmospheric Chemistry and Physics*, 10(13), 5999–6006. https://doi.org/10.5194/acp-10-5999-2010
- Kravitz, B., Lamarque, J.-F., Tribbia, J. J., Tilmes, S., Vitt, F., Richter, J. H., et al. (2017). First simulations of designing stratospheric sulfate aerosol geoengineering to meet multiple simultaneous climate objectives. *Journal of Geophysical Research: Atmospheres*, 122(23), 12616–12634. https://doi.org/10.1002/2017jd026874
- Kravitz, B., MacMartin, D. G., Wang, H., & Rasch, P. J. (2016). Geoengineering as a design problem. Earth System Dynamics, 7(2), 469–497. https://doi.org/10.5194/esd-7-469-2016
- Laakso, A., Kokkola, H., Partanen, A.-I., Niemeier, U., Timmreck, C., Lehtinen, K. E. J., et al. (2016). Radiative and climate impacts of a large volcanic eruption during stratospheric sulfur geoengineering. Atmospheric Chemistry and Physics, 16(1), 305–323. https://doi.org/10.5194/acp-16-305-2016
- Lee, W., MacMartin, D., Visioni, D., & Kravitz, B. (2020). Expanding the design space of stratospheric aerosol geoengineering to include precipitation-based objectives and explore trade-offs. Earth System Dynamics, 11(4), 1051–1072. https://doi.org/10.5194/esd-11-1051-2020
- Liu, X., Ma, P.-L., Wang, H., Tilmes, S., Singh, B., Easter, R. C., et al. (2016). Description and evaluation of a new four-mode version of the Modal Aerosol Module (MAM4) within version 5.3 of the community atmosphere model. *Geoscientific Model Development*, 9(2), 505–522. https://doi.org/10.5194/gmd-9-505-2016
- MacMartin, D. G., Caldeira, K., & Keith, D. W. (2014). Solar geoengineering to limit the rate of temperature change. Philosophical Transactions of the Royal Society A: Mathematical, Physical & Engineering Sciences, 372(2031), 20140134. https://doi.org/10.1098/rsta.2014.0134
- MacMartin, D. G., Kravitz, B., Mills, M. J., Tribbia, J. J., Tilmes, S., Richter, J. H., et al. (2017). The climate response to stratospheric aerosol geoengineering can be tailored using multiple injection locations. *Journal of Geophysical Research: Atmospheres*, 122(23), 12574–12590. https://doi.org/10.1002/2017jd026868
- MacMartin, D. G., Ricke, K. L., & Keith, D. W. (2018). Solar geoengineering as part of an overall strategy for meeting the 1.5°C Paris target. Philosophical Transactions of the Royal Society A: Mathematical, Physical & Engineering Sciences, 376(2119), 20160454. https://doi.org/10.1098/rsta.2016.0454

QUAGLIA ET AL. 11 of 12



- 10.1029/2023GL107702
- MacMartin, D. G., Visioni, D., Kravitz, B., Richter, J., Felgenhauer, T., Lee, W. R., et al. (2022). Scenarios for modeling solar radiation modification. Proceedings of the National Academy of Sciences of the United States of America, 119(33), e2202230119. https://doi.org/10.1073/pnas.2202230119
- Marshall, L. R., Maters, E. C., Schmidt, A., Timmreck, C., Robock, A., & Toohey, M. (2022). Volcanic effects on climate: Recent advances and future avenues. Bulletin of Volcanology, 84(5), 54. https://doi.org/10.1007/s00445-022-01559-3
- Meinshausen, M., Nicholls, Z. R. J., Lewis, J., Gidden, M. J., Vogel, E., Freund, M., et al. (2020). The shared socio-economic pathway (SSP) greenhouse gas concentrations and their extensions to 2500. Geoscientific Model Development, 13(8), 3571–3605. https://doi.org/10.5194/gmd-13-3571-2020
- Mills, M. J., Richter, J. H., Tilmes, S., Kravitz, B., MacMartin, D. G., Glanville, A. A., et al. (2017). Radiative and chemical response to interactive stratospheric sulfate aerosols in fully coupled CESM1(WACCM). *Journal of Geophysical Research: Atmospheres*, 122(23), 13061–13078. https://doi.org/10.1002/2017JD027006
- Oman, L., Robock, A., Stenchikov, G. L., Thordarson, T., Koch, D., Shindell, D. T., & Gao, C. (2006). Modeling the distribution of the volcanic aerosol cloud from the 1783–1784 Laki eruption. *Journal of Geophysical Research*, 111(D12), D12209. https://doi.org/10.1029/ 2005JD006899
- Quaglia, I. (2023). Data from: The potential of Stratospheric Aerosol Injection to reduce the climatic risks of explosive volcanic eruptions [Dataset]. Zenodo. https://doi.org/10.5281/zenodo.10257628
- Ricke, K. L., Millar, R. J., & MacMartin, D. G. (2017). Constraints on global temperature target overshoot. Scientific Reports, 7(1), 14743. https://doi.org/10.1038/s41598-017-14503-9
- Ridley, H. E., Asmerom, Y., Baldini, J. U. L., Breitenbach, S. F. M., Aquino, V. V., Prufer, K. M., et al. (2015). Aerosol forcing of the position of the intertropical convergence zone since ad 1550. Nature Geoscience, 8(3), 195–200. https://doi.org/10.1038/ngeo2353
- Robock, A. (2000). Volcanic eruptions and climate. Reviews of Geophysics, 38(2), 191-219. https://doi.org/10.1029/1998RG000054
- Schmidt, A., Mills, M. J., Ghan, S., Gregory, J. M., Allan, R. P., Andrews, T., et al. (2018). Volcanic radiative forcing from 1979 to 2015. *Journal of Geophysical Research: Atmospheres*, 123(22), 12491–12508. https://doi.org/10.1029/2018JD028776
- Schoeberl, M. R., Wang, Y., Ueyama, R., Taha, G., & Yu, W. (2023). The cross equatorial transport of the Hunga Tonga-Hunga Ha'apai eruption plume. Geophysical Research Letters, 50(4), e2022GL102443. https://doi.org/10.1029/2022GL102443
- Self, S. (2006). The effects and consequences of very large explosive volcanic eruptions. *Philosophical Transactions of the Royal Society A: Mathematical, Physical & Engineering Sciences, 364*(1845), 2073–2097. https://doi.org/10.1098/rsta.2006.1814
- Soden, B. J., Wetherald, R. T., Stenchikov, G. L., & Robock, A. (2002). Global cooling after the eruption of Mount Pinatubo: A test of climate feedback by water vapor. Science, 296(5568), 727–730. https://doi.org/10.1126/science.296.5568.727
- Tang, A., & Kemp, L. (2021). A fate worse than warming? Stratospheric aerosol injection and global catastrophic risk. Frontiers in Climate, 3. https://doi.org/10.3389/fclim.2021.720312
- Textor, C., Graf, H.-F., Timmreck, C., & Robock, A. (2004). Emissions from volcanoes. Advances in Global Change Research, 18, 269–303. https://doi.org/10.1007/978-1-4020-2167-1\_7
- Timmreck, C., Graf, H.-F., Zanchettin, D., Hagemann, S., Kleinen, T., & Krüger, K. (2012). Climate response to the Toba super-eruption: Regional changes. *Quaternary International*, 258, 30–44. https://doi.org/10.1016/j.quaint.2011.10.008
- Trenberth, K. E., & Dai, A. (2007). Effects of Mount Pinatubo volcanic eruption on the hydrological cycle as an analog of geoengineering: Pinatubo and the hydrological cycle. *Geophysical Research Letters*, 34(15), L15702. https://doi.org/10.1029/2007GL030524
- Visioni, D., MacMartin, D. G., Kravitz, B., Tilmes, S., Mills, M. J., Richter, J. H., & Boudreau, M. P. (2019). Seasonal injection strategies for stratospheric aerosol geoengineering. Geophysical Research Letters, 46(13), 7790–7799. https://doi.org/10.1029/2019GL083680
- Yang, W., Vecchi, G. A., Fueglistaler, S., Horowitz, L. W., Luet, D. J., Muñoz, A. G., et al. (2019). Climate impacts from large volcanic eruptions in a high-resolution climate model: The importance of forcing structure. *Geophysical Research Letters*, 46(13), 7690–7699. https://doi.org/10.1029/2019GL082367
- Yu, F., Luo, G., Nair, A. A., Eastham, S., Williamson, C. J., Kupc, A., & Brock, C. A. (2023). Particle number concentrations and size distributions in the stratosphere: Implications of nucleation mechanisms and particle microphysics. *Atmospheric Chemistry and Physics*, 23(3), 1863–1877. https://doi.org/10.5194/acp-23-1863-2023
- Zuo, M., Zhou, T., & Man, W. (2019). Hydroclimate responses over global monsoon regions following volcanic eruptions at different latitudes. *Journal of Climate*, 32(14), 4367–4385. https://doi.org/10.1175/JCLI-D-18-0707.1

QUAGLIA ET AL. 12 of 12